

Observation of a Long-Wavelength Hosing Modulation of a High-Intensity Laser Pulse in Underdense Plasma

M. C. Kaluza^{1,2,3}, S. P. D. Mangles¹, A. G. R. Thomas^{1,4}, Z. Najmudin¹, A. E. Dangor¹, C. D. Murphy^{1,5,6}, J. L. Collier⁵, E. J. Divall⁵, P. S. Foster⁵, C. J. Hooker⁵, A. J. Langley⁵, J. Smith⁵, and K. Krushelnick^{1,4}

¹*The Blackett Laboratory, Imperial College London SW7 2AZ, United Kingdom*

²*Institut für Optik und Quantenelektronik, Friedrich-Schiller-Universität, Max-Wien-Platz 1, 07743 Jena, Germany*

³*Helmholtz-Institut Jena, Helmholtzweg 4, 07743 Jena, Germany*

⁴*Center for Ultrafast Optical Science (CUOS), University of Michigan, Ann Arbor, Michigan 48109, USA*

⁵*Central Laser Facility, Rutherford Appleton Laboratory, Oxon OX11 0QX, United Kingdom and*

⁶*Clarendon Laboratory, University of Oxford, Oxford OX1 3PU, United Kingdom*

We report the first experimental observation of a long-wavelength hosing modulation of a high-intensity laser pulse. Side-view images of the scattered optical radiation at the fundamental wavelength of the laser reveal a transverse oscillation of the laser pulse during its propagation through underdense plasma. The wavelength of the oscillation λ_{hosing} depends on the background plasma density n_e and scales as $\lambda_{\text{hosing}} \sim n_e^{-3/2}$. Comparisons with an analytical model and 2-dimensional particle-in-cell simulations reveal that this laser hosing can be induced by a spatio-temporal asymmetry of the intensity distribution in the laser focus which can be caused by a misalignment of the parabolic focussing mirror or of the diffraction gratings in the pulse compressor.

PACS numbers: 52.38.Kd, 41.75.Jv, 29.30.Ep

Since the first theoretical prediction [1] and experimental observation [2–4] of laser-accelerated electron pulses showing a narrow energy spread, the prospect of a tabletop laser-based particle accelerator has come closer to reality. Such an electron source would allow for the generation of THz-radiation [5], a high-intensity, narrowband femtosecond source of visible or X-ray radiation [6, 7], and possibly a free-electron laser in a university-scale laboratory. However, for all these applications a high degree of stability and reproducibility of the electron pulse is mandatory. This is difficult to achieve due to the inherently non-linear processes involved in the generation of quasi-monoenergetic electrons. Here, the ponderomotive potential of the high-intensity laser pulse excites a plasma wave. Feedback between laser and plasma wave induces longitudinal and transverse modulation of the laser pulse and non-linear steepening of the wave. When the wave eventually breaks plasma electrons are injected into the electric field associated with the wave (the “wake field”) [8] which can accelerate them to relativistic energies.

To improve the stability of the electron beam, preionized plasma channels [9, 10] or gas-filled capillaries [11] have been used. Additionally, improving the laser contrast [12] and using two counter-propagation pulses [13] has increased the energy and pointing stability of the electrons. However, asymmetries in the spatio-temporal profile of the focussed laser pulse or of the initial plasma distribution have been shown for pulses significantly longer than the plasma wavelength to significantly affect the propagation of the laser through the plasma and eventually influence the interaction [14–17]. Furthermore, the propagation of two separated focal spots can be interlinked via the plasma acting as a non-linear medium initiating a braided motion of the two focal spots

[18]. Thus it is crucial to gain as much information on the interaction process and about influences of experimental parameters that can significantly affect the interaction and eventually the electron-bunch generation.

In this Letter, we show for the first time that also a laser pulse with a length of the order of the plasma wavelength exhibiting a distinctly asymmetric far-field intensity distribution can trigger a hosing modulation leading to transverse oscillations of the pulse during its propagation through the plasma. The wavelength of this hosing strongly depends on the background plasma density.

The experiments were carried out using the 10-TW Ti:Sapphire laser system ASTRA at the Rutherford Appleton Laboratory. 45-fs, 350-mJ laser pulses at a central wavelength of $\lambda_L = 800$ nm were focussed into the leading edge of a supersonic He-gas jet produced by a conical nozzle having an exit diameter of 2 mm. This gas jet exhibited an almost flat-top longitudinal density profile as characterized before the experiment. The density in the plateau region could be adjusted by changing the backing pressure. Assuming full ionization the corresponding plasma densities were between $n_e = 4 \times 10^{18}$ and $4 \times 10^{19} \text{ cm}^{-3}$. The horizontally polarized laser pulses were focussed by an $f/16$ off-axis parabolic mirror to a focal spot with a diameter of $30 \mu\text{m}$, the intensity averaged within this area was $1.2 \times 10^{18} \text{ W/cm}^2$. The fluence profile of the focussed laser pulses was strongly attenuated and imaged onto a CCD camera. During the full-power shots, the pointing and an equivalent fluence distribution of the far-field of the laser could be monitored by imaging the leakage of the laser through the last plane mirror in front of the parabola using an $f/20$ -lens and a CCD. Looking in the direction of laser polarization the interaction region in the plasma was imaged using a

high-quality $f/2$ -lens with a magnification of 10 onto a 12-bit CCD camera equipped with an interference filter transmitting at (800 ± 10) nm. The spatial resolution was close to $2 \mu\text{m}$, the field of view in the interaction region was $540 \mu\text{m} \times 400 \mu\text{m}$. MeV-electrons generated during the interaction could be detected by an electron beam monitor consisting of a CCD camera looking at a fluorescent screen positioned 480 mm behind the target and shielded by 20 mm thick aluminium making it sensitive to electrons with $E_{\text{kin}} \geq 11$ MeV. Furthermore, the spectra of the electrons could be measured using a high-resolution magnetic spectrometer equipped with imaging plate detectors. The electron spectra exhibited quasi-monoenergetic features.

Fig. 1 shows four images of the scattered light recorded at the fundamental wavelength by the side-view imaging system. All images show a field-of-view

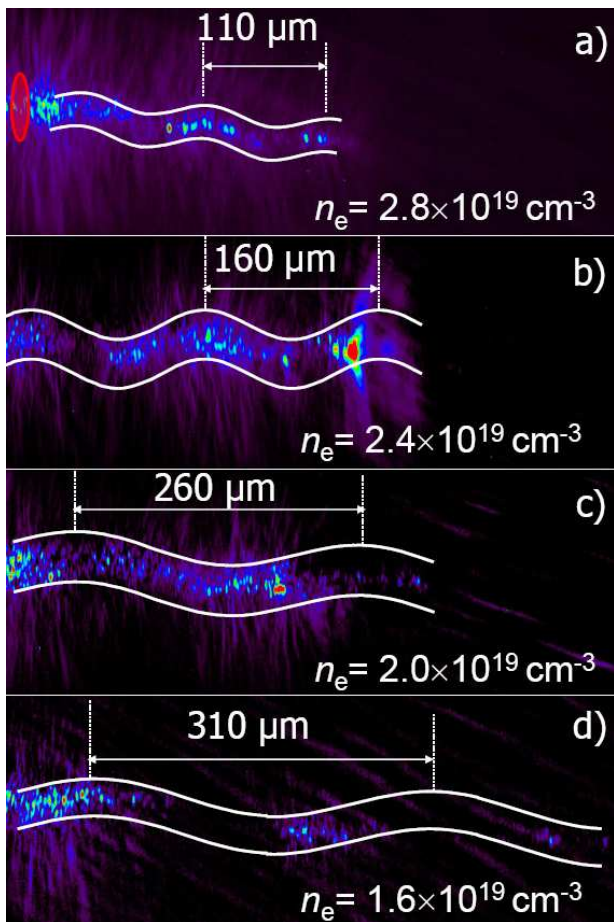


FIG. 1: Side-view images of the electromagnetic radiation scattered from the plasma at λ_L . The images have a size of $500 \mu\text{m} \times 100 \mu\text{m}$ and have been stretched vertically by a factor of 2. The laser pulse shows a hosing-type transverse oscillation, highlighted by the white lines. The hosing wavelength continuously increases with decreasing plasma density n_e .

of $500 \mu\text{m} \times 100 \mu\text{m}$. Note that they have been stretched

vertically by a factor of 2. The initial plasma densities in these four images were $n_e = 2.8$ (a), 2.4 (b), 2.0 (c), and $1.6 \times 10^{19} \text{ cm}^{-3}$ (d), respectively. All images have been filtered differently to record similar dynamic ranges for different levels of the scattered light.

The laser pulse (propagating left to right) was focused into the leading edge of the gas jet located close to the left boundary of each image. The red ellipse in Fig. 1 a) depicts the size and approximate position of the vacuum laser focus. As the laser power is high enough to trigger relativistic self-focussing (the critical power for a density of $n_e = 2.8 \times 10^{19} \text{ cm}^{-3}$ is 1.2 TW, well below our laser power), the transverse diameter of the laser pulse decreased during its propagation through the plasma. Note that since the radiation is only scattered from the plasma electrons at the instantaneous position of the laser pulse in the plasma, each image represents a history of the instantaneous position of the laser as a function of propagation distance. Hence, the horizontal axis represents both distance and time of propagation.

Furthermore, it is obvious in all four images that the laser pulse does not propagate on a straight line but carries out transverse hosing-type oscillations. While the amplitude of the oscillation of a few μm remains approximately constant both during the propagation and for the different background densities, the wavelength of this hosing modulation significantly increases with decreasing plasma density from $(110 \pm 25) \mu\text{m}$ for the highest density up to $(310 \pm 50) \mu\text{m}$ for the lowest. This is summarized in Fig. 2. Note that due to the decreasing plasma density

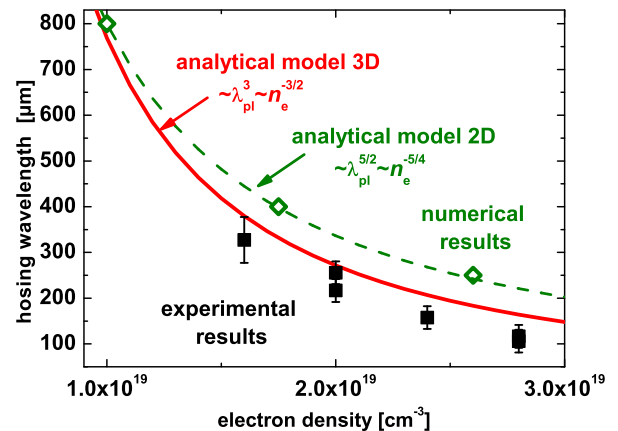


FIG. 2: Dependence of the hosing wavelength λ_{hosing} on the electron density n_e for the experiment (black solid squares) and for the results from the numerical simulation (green open diamonds). These results are compared to predictions by an analytical model scaling like $\lambda_{\text{hosing}} \sim n_e^{-3/2}$ in 3D (red line) and like $\lambda_{\text{hosing}} \sim n_e^{-5/4}$ in 2D (green line).

the intensity of the scattered light decreases, since the scattering is directly proportional to the number of free electrons. It had decreased below our detection threshold

for even lower densities.

The long-wavelength hosing modulation observed in our experiment is very likely to be caused by the focal spot of the laser pulse exhibiting a spatio-temporal asymmetry in its intensity distribution relative to the phase fronts of the pulse. This asymmetry can arise due to a variety of reasons in a chirped pulse amplification laser system, such as by a slight misalignment of the parabolic focussing mirror, a slight misalignment of the diffraction gratings used to compress the pulse after amplification, pointing fluctuations of the laser pulse itself induced by mechanical vibrations or air turbulences or a combination of these effects. Due to a feedback mechanism be-

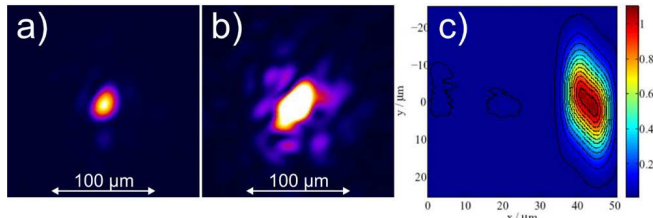


FIG. 3: Energy-density profile of the laser far-field at two different filter levels, a) and b). Snapshot of the initial, asymmetric laser-intensity profile used in the simulations, c).

tween the intensity distribution of the laser pulse and the plasma density mediated by the local refractive index of the plasma, $\eta(\mathbf{r}) = (1 - n_e(\mathbf{r})/n_{cr})^{1/2}$, and the ponderomotive potential of the laser, the propagation of the laser pulse is strongly influenced by the plasma density distribution. Here, $n_{cr} = \omega_L^2 \epsilon_0 m_e / e^2 = 4\pi^2 \epsilon_0 m_e c^2 / e^2 \lambda_L^2$ is the critical density of the plasma for the wavelength λ_L and frequency ω_L of the laser light, ϵ_0 is the dielectric constant and e and m_e are the electron charge and mass, respectively. The gradient of the plasma's refractive index initiated by the head of the pulse via its ponderomotive potential will be asymmetric with respect to the bulk of the pulse, and will therefore provide an effective focussing “force”. This exerts a transverse, restoring force on the bulk of the pulse, causing this part of the pulse to execute transverse oscillations. Typical, slightly asymmetric laser foci measured during the experiment with different filter levels are shown in Fig. 3 a) and b). Note that both images show a time-integrated measurement of the intensity distribution, i.e. the laser fluence in the focal plane. Under conditions where no such focal spot asymmetry was present, no hosing modulation could be detected.

To verify this hypothesis, we carried out 2-dimensional Particle-In-Cell (2D-PIC) simulations using the code OSIRIS [19] starting with an asymmetric laser pulse. The spatio-temporal pulse intensity profile used in our simulations, as shown in Fig. 3 c) was achieved by overlapping two laser pulses of equal intensity, both having a radius of $10 \mu\text{m}$ ($1/e^2$ in intensity) mimicking the focal-

spot asymmetry in the experiment. The two parts of the pulse were separated both in longitudinal (i.e. in propagation direction) and in transverse direction by $6\lambda_L$. They were overlapped at focus, so that the phase fronts were flat. This resulted in a smooth pulse profile despite being constructed of two pulses. The size of each part of the focal spot in the simulation was chosen as $w_0 = 10 \mu\text{m}$, which is slightly smaller than in the experiment to account for the under-estimated self-focussing in 2D simulations. Accordingly, $a_0 = 1.5$ was chosen higher than in the experiment. Fig. 4 (a)-(c) show the numerical results obtained for three different densities. It is obvious

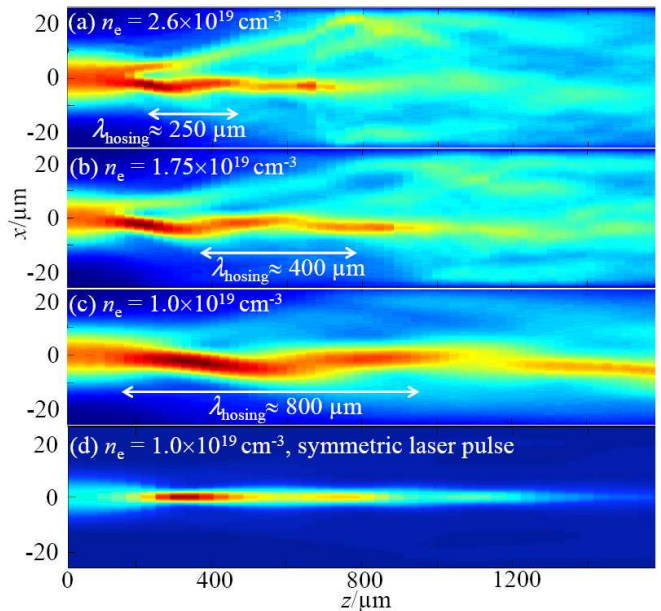


FIG. 4: Numerically simulated propagation of the laser pulse in the plasma. The images show the energy-density distribution of the scattered light at the fundamental wavelength in transverse direction for electron plasma densities of $2.6 \times 10^{19} \text{ cm}^{-3}$ (a), $1.75 \times 10^{19} \text{ cm}^{-3}$ (b), and $1.0 \times 10^{19} \text{ cm}^{-3}$ (c) and (d). The corresponding hosing wavelengths are also indicated. No hosing occurs for a symmetric laser pulse (d).

that the propagation of the laser pulse shows a transverse hosing modulation, with amplitude and wavelength similar to the experiment as also shown in Fig. 2. Fig. 4 (d) shows the result for similar parameters as in (c) but for a pulse exhibiting no spatio-temporal asymmetry. In this case no hosing occurs.

A heuristic description of the interaction can be found by assuming that the bulk of the pulse resides in the quasi-static wake generated by the head of the pulse due to its ponderomotive force. The general approach is to assume the pulse is weakly relativistic, so that a density depression but not complete cavitation is generated by the pulse-front. The bulk of the pulse, displaced transversely to the propagation direction with respect to the

head of the pulse, experiences the refractive index gradient associated with the density depression. This acts to direct the pulse energy towards the axis.

By considering the bending of phase fronts of the bulk of the pulse analogous to [20], the position of the centroid of the bulk of the pulse, $\langle r \rangle$, with respect to the radially varying plasma density induced by the front of the pulse, neglecting longitudinal dynamics, can be expressed as

$$\frac{\partial^2}{\partial t^2} \langle r \rangle \approx -\frac{c^2}{2} \frac{\partial}{\partial r} \left(\frac{\delta n_e}{n_{cr}} \right). \quad (1)$$

Assuming an approximate balance between the ponderomotive and wakefield potentials for a weakly relativistic pulse, the density perturbation can be expressed as $\delta n_e/n_{cr} \approx (c^2/\omega_L^2)\nabla^2 a^2/4$. If the field strength is distributed as $a(r)^2 = a_0^2(w_0^2/w^2) \cos(\pi r/2w)$, where w_0 and $a_0 = eE_0/(m_e c \omega_L)$ are the initial pulse-front radius and the normalized amplitude of the vector potential, respectively (E_0 is the amplitude of the laser's electric field), and w is the radius of the front of the pulse after self-focussing, then $\delta n_e/n_{cr} \approx -(a_0^2 w_0^2 \pi^2 c^2 / 16 \omega_L^2 w^4) \cos(\pi r/2w)$. The expression for the field strength neglects absorption of pulse energy which conserves laser power, $a_0 w_0 = a w$. We will assume that the pulse asymmetry lies in the $x-z$ plane so that the oscillations will occur in the x -direction. Hence, for the bulk of the pulse the equation for the centroid position is now

$$\frac{\partial^2}{\partial t^2} \langle x \rangle \approx -\frac{a_0^2 w_0^2 \pi^3 c^4}{64 \omega_L^2 w^5} \sin\left(\frac{\pi}{2w} \langle x \rangle\right). \quad (2)$$

To first order in $\langle x \rangle$, this is a harmonic oscillator equation with a frequency $\omega_{\text{hosing}} \approx a_0 w_0 \pi^2 c^2 / (8\sqrt{2} \omega_L w^3)$. Using this frequency of oscillation, the expression yields $\lambda_{\text{hosing}} \approx 16\sqrt{2} \omega_L w^3 / (a_0 w_0 \pi c)$. For a weakly relativistic pulse, the pulse self-focusses to a radius of approximately half the plasma wavelength, $w \approx \pi c / \omega_p$ [21], leading to

$$\lambda_{\text{hosing}} \approx \frac{4\sqrt{2} \lambda_L^2}{a_0 w_0} \left(\frac{n_{cr}}{n_e} \right)^{3/2}. \quad (3)$$

For initial pulse radius and field strength $w_0 = 15 \mu\text{m}$, $a_0 = 0.75$, respectively, and $\lambda_L = 0.8 \mu\text{m}$, a hosing wavelength of $\lambda_{\text{hosing}} = 0.32 \mu\text{m} \cdot (n_{cr}/n_e)^{3/2}$ is obtained. This agrees well with the experiment as shown by the red line in Fig. 2. For the simulations, in a 2D slab geometry, the expression for constant power is $a_0^2 w_0 = a^2 w$. This modifies the hosing wavelength to be $\lambda_{\text{hosing,2D}} \approx 8\lambda_L^{3/2} / (a_0 \sqrt{w_0}) (n_{cr}/n_e)^{5/4}$, which explains the slightly different scaling. Using $w_0 = 10 \mu\text{m}$, $a_0 = 1.5$ gives the dashed green line in Fig. 2, which shows excellent agreement between the model and the 2D-simulation data.

In conclusion, we have observed the transverse hosing-type oscillation of an ultra-short laser pulse during its

propagation through underdense plasma. Analytical estimates and 2D-PIC simulations have shown that such a transverse oscillation can be caused by a spatio-temporal asymmetry of the intensity of the laser pulse. For experiments towards the generation and application of collimated, quasi-monoenergetic electron pulses where stability is an important issue, such transverse oscillations of the laser pulse are likely to influence the electron acceleration process. To improve the stability of the electron pulse it is necessary to carefully control and monitor the spatio-temporal characteristic of the driving laser pulse. It is conceivable that the hosing modulation will become more pronounced at higher laser powers as in this case the sensitivity to phase front tilts is likely to be higher. Deliberately exciting hosing of this form could also have a significant effect on x-rays produced by betatron oscillations which has been shown to be sensitive to focal spot asymmetries [22].

This work has been supported by the BMBF (contract no. 03ZIK052) and by the DFG (contract no. TR18). S.P.D.M. thanks the Royal Society for support and A.G.R.T. was supported by the NSF under contract 0903557. We also thank the OSIRIS Consortium.

-
- [1] A. Pukhov and J. Meyer-ter-Vehn, *Appl. Phys. B* **74**, 355 (2002).
 - [2] S. P. D. Mangles *et al.*, *Nature* **431**, 535 (2004).
 - [3] C. G. R. Geddes *et al.*, *Nature* **431**, 538 (2004).
 - [4] J. Faure *et al.*, *Nature* **431**, 541 (2004).
 - [5] W. P. Leemans *et al.*, *Phys. Rev. Lett.* **91**, 074802 (2003).
 - [6] H.-P. Schlenvoigt *et al.*, *Nature Phys.* **2**, 135005 (2008).
 - [7] A. Rousse *et al.*, *Phys. Rev. Lett.* **93**, 135005 (2004).
 - [8] M. C. Kaluza *et al.*, submitted (2010).
 - [9] W. P. Leemans *et al.*, *Nature Phys.* **2**, 696 (2006).
 - [10] S. Karsch *et al.*, *New J. Phys.* **2**, 696 (2007).
 - [11] J. Osterhoff *et al.*, *Phys. Rev. Lett.* **101**, 085002 (2008).
 - [12] S. P. D. Mangles *et al.*, *Plasma Phys. Control. Fusion* **48**, B83 (2006).
 - [13] J. Faure *et al.*, *Nature* **444**, 737 (2006).
 - [14] G. Shvets and J. S. Wurtele, *Phys. Rev. Lett.* **73**, 3540 (1994).
 - [15] P. Sprangle *et al.*, *Phys. Rev. Lett.* **73**, 3544 (1994).
 - [16] B. J. Duda *et al.*, *Phys. Rev. Lett.* **83**, 1978 (1999).
 - [17] Z. Najmudin *et al.*, *Phys. Plasmas* **10**, 438 (2003).
 - [18] C. Ren *et al.*, *Phys. Rev. Lett.* **85**, 2124 (2000).
 - [19] R. A. Fonseca *et al.* *Lecture Notes in Computer Science* Vol. **2329**, III-342 (Springer, Heidelberg, 2002).
 - [20] W. B. Mori, *IEEE J. Quantum Electron.* **33**, 1942 (1997).
 - [21] A. G. R. Thomas *et al.*, *Phys. Rev. Lett.* **98**, 095004 (2007).
 - [22] S. P. D. Mangles *et al.*, *Appl. Phys. Lett.* **95**, 181106 (2009).